Available online at www.sciencedirect.com
SCIENCE DIRECT®
International Journal of Thermal Sciences 42 (2003) 481–498
International Journal of Thermal Sciences
www.elsevier.com/locate/ijts

Character and stability of a wind-driven supercooled water film on an icing surface—I. Laminar heat transfer

A.R. Karev [a], M. Farzaneh [a,*], E.P. Lozowski [b]

[a] *NSERC/Hydro-Québec/UQAC Industrial Chair on Atmospheric Icing of Power Network Equipment (CIGELE), Université du Québec à Chicoutimi, 555 Boulevard de l'Université, Chicoutimi, PQ, Canada G7H 2B1*
[b] *Department of Earth and Atmospheric Sciences, University of Alberta, Edmonton, AB, Canada T6G 2E3*

Received 13 February 2002; accepted 18 June 2002

Abstract

The kinetics of freezing of a supercooled water film flowing on an icing surface is considered here for the case of laminar heat transfer through the water film. The linear growth rate of crystallization (LRC) in a supercooled, laminar water film, flowing over an accreting ice surface, is found to be characterized by unique behaviours at different length scales. The icing surface is envisaged as a semi-infinite horizontal flat plate with vertically impinging supercooled water droplets. The water film begins to develop at the edge of the plate and thickens while it collects impinging water as the horizontal wind stress drives it downstream. At very short distances from the Couette flow origin, where convection prevails over conduction through the water film, the LRC reacts in a stable fashion to instantaneous changes in the external thermodynamic parameters. The LRC accelerates or decelerates, responding to variations in the water film thickness. At intermediate distances from the flow origin, the LRC is independent of sudden perturbations in the water film thickness, and is determined only by the mean external parameters that characterize the heat transfer and flow dynamics at the water film surface. At a still greater distance from the flow origin, the LRC is unstable in a shear-driven, supercooled water film, flowing over an accreting ice surface. The instability gives rise to either complete disappearance of the water film or a total change of the momentum and heat transfer regime.

Keywords: Supercooled water film; Ice accretion; Linear rate of crystallization; Laminar Couette flow

1. Introduction

The traditional conceptual model of the icing process on a structure embedded within a supercooled aerosol stream consists of two parts:

(i) the aerodynamic theory of the flow of the aerosol particles around the structure—[1,2], and,
(ii) a thermodynamic heat balance calculation at its surface which determines the accretion rate—[3–5].

Without denying the importance of the former, the present work deals only with the thermodynamic aspects of the icing process. In it, we will try to elucidate the processes at work in a wind-sheared supercooled liquid film flowing on an icing surface, and to investigate how these processes might govern the rate of ice formation.

1.1. Wet and dry modes of ice growth

The current approach to considering the icing heat balance is a macroscopic one, developed originally for the purpose of aircraft icing modelling [3]. In this approach, for the purpose of calculating the temperature of an icing surface, the temperature of fusion, $T_m = 273.15$ K, is taken as the reference point, distinguishing the solid and liquid states of water. An examination of the heat balance relative to this reference point is accomplished by the introduction of a freezing fraction coefficient, defined as the fraction of the impinging aerosol mass that turns into ice. When the freezing fraction is less than unity, the remaining unfrozen liquid is assumed to form a water film on the icing surface, which moves under the influence of aerodynamic and gravitational forces. This liquid film can play a significant role in the heat and mass transfer processes. The icing regime with such a liq-

* Corresponding author.
E-mail address: farzaneh@uqac.uquebec.ca (M. Farzaneh).
URL address: http://icevolt.uqac.uquebec.ca/cigele.

1290-0729/02/$ – see front matter
doi:10.1016/S1290-0729(02)00049-2

Nomenclature

a empirical constant (see (9)) ..... $\mathrm{m\cdot s^{-1}\cdot K^{-b}}$
b empirical constant in the formula for linear rate of crystallization (see (9))
A dendrite curvature ratio (see (36))
c_f skin friction coefficient
c_w specific heat capacity of water .... $\mathrm{J\cdot kg^{-1}\cdot K^{-1}}$
C constant, $= 0.6 \times 10^{-6}$ ..... $\mathrm{m\cdot K}$
C_e correction to the rate of displacement of the air/water surface due to evaporation .... $\mathrm{m\cdot s^{-1}}$
$\overline{E}$ mean transfer efficiency of the dispersed phase from the aerosol onto the surface of the water film
f dimensionless function in the similarity transformation
f_i interfacial friction factor
F interfacial shear stress applied to the surface of the water film ..... $\mathrm{N\cdot m^{-2}}$
g acceleration due to gravity ..... $\mathrm{m\cdot s^{-2}}$
G_a ice growth rate along the a-axis ..... $\mathrm{m\cdot s^{-1}}$
G_c ice growth rate along the c-axis ..... $\mathrm{m\cdot s^{-1}}$
G_m maximum ice growth rate ..... $\mathrm{m\cdot s^{-1}}$
h water film thickness ..... m
h_{eq} equilibrium water film thickness, defined by equating $\mathrm{d}y_1/\mathrm{d}\tau$ and $\mathrm{d}y_2/\mathrm{d}\tau$ (see (41)) ..... m
$h_{g\nu}$ water film thickness characterizing the interaction between gravity and viscosity, $= (\frac{\nu_w^2 \rho_w}{g(\rho_w - \rho_a)})^{1/3} \cong (\frac{\nu_w^2}{g})^{1/3}$ ..... m
H dimensional coefficient of heat transfer to water film ..... $\mathrm{W\cdot m^{-2}\cdot K^{-1}}$
$H^+ = Nu^*$ dimensionless coefficient of heat transfer to water film
k_s height of the roughness elements ..... m
l plate length ..... m
L_i specific latent heat of freezing of water . $\mathrm{J\cdot kg^{-1}}$
Pr and Pr_t molecular and turbulent Prandtl numbers for water, respectively
$Q_{\mathrm{out},s}$ net heat flux at the surface of the water film ..... $\mathrm{W\cdot m^{-2}}$
Q_{wl} heat flux at the ice/water interface ..... $\mathrm{W\cdot m^{-2}}$
R_C and R_2 principal and secondary radii of curvature of the tip of an ice dendrite, respectively, ... m
Re Reynolds number
$T(x, y)$ temperature field in the supercooled water film ..... K
T_m temperature of fusion of water, $= 273.15$.... K
$\overline{T'v'}$ turbulent heat flux, time averaged product of T' and v' ..... $\mathrm{m\cdot K\cdot s^{-1}}$
$u(y)$ and $v(y)$ tangential and normal components of water film velocity ..... $\mathrm{m\cdot s^{-1}}$
$\overline{u'v'}$ turbulent "shear stress", time averaged product of u' and v' ..... $\mathrm{m^2\cdot s^{-2}}$
u_{w-a} friction velocity at the air/water interface $\mathrm{m\cdot s^{-1}}$
w liquid water content (LWC) of the air-aerosol flow ..... $\mathrm{kg\cdot m^{-3}}$
x and y tangential and normal co-ordinates in the water film, respectively ..... m
$\frac{\mathrm{d}y_1}{\mathrm{d}\tau}$ rate of macroscopic displacement of the ice/water interface ..... $\mathrm{m\cdot s^{-1}}$
$\frac{\mathrm{d}y_2}{\mathrm{d}\tau}$ rate of displacement of the air/water interface ..... $\mathrm{m\cdot s^{-1}}$

Greek symbols

$\alpha = 1.3282$ constant arising from the similarity transformation (see (26))
δ_T and δ_D laminar thermal and dynamic boundary layer thicknesses, respectively ..... m
Δ_1 $= T_m - T_1$ supercooling at the ice/water interface ..... K
Δ_2 $= T_m - T_2$ supercooling at the air/water interface ..... K
Δ_{bk} $= \frac{1}{h}\int_0^h (T_m - T)\,\mathrm{d}y = f(\Delta_1, \Delta_2, h)$ supercooling of the bulk water ..... K
φ inclination of the dendrites with respect to the basal plane
ε_M and ε_H eddy diffusivity of water for momentum and heat transfer ..... $\mathrm{m^2\cdot s^{-1}}$
ζ dimensionless variable (see (29))
η dimensionless coordinate arising from the similarity transformation (see (20))
Θ dimensionless temperature, $= \frac{T_1 - T}{T_1 - T_2}$
λ_w thermal conductivity of water .... $\mathrm{W\cdot m^{-1}\cdot K^{-1}}$
Λ similarity variable, $= \nu_w(\frac{\rho_w x}{F\cdot h})^{1/2}$ ..... m
ν_a kinematic viscosity of air ..... $\mathrm{m^2\cdot s^{-1}}$
ν_w kinematic viscosity of water ..... $\mathrm{m^2\cdot s^{-1}}$
ρ_a air density ..... $\mathrm{kg\cdot m^{-3}}$
ρ_i density of the growing ice layer at the interface y_1 ..... $\mathrm{kg\cdot m^{-3}}$
ρ_w water density ..... $\mathrm{kg\cdot m^{-3}}$
τ time ..... s
χ_w thermal diffusivity of water ..... $\mathrm{m^2\cdot s^{-1}}$
ψ stream function for components of velocity in the water film ..... $\mathrm{m^2\cdot s^{-1}}$

Subscripts

1 ice/water planar interface
2 and s air/water interface
bk bulk
a air
crit critical
F film
FL flow
eq equilibrium
i ice
l laminar

lin	linear	w	water
s	surface	*Superscript*	
SH	shear stress	$+, *$	dimensionless
t	turbulent		

uid film is typically referred to as "wet". The "dry" regime, when the freezing fraction equals unity, is characterized by the complete freezing of the impinging water without the formation of a liquid film.[1] We ignore, for now, the possibility of spongy ice formation.

A series of experiments with artificial hailstones grown under laboratory conditions simulating natural conditions, [9] and [10], has confirmed that the temperature of the water film on an icing surface in the wet mode is always below 0 °C. This observation suggests the need to propose an alternative to the traditional macroscopic approach, for distinguishing between icing growth regimes with and without a water film on an icing surface. The terminologies "wet" and "dry" applied for this distinction in various models of ice accretion since the time of Schumann's theoretical work [4], are becoming obsolete and misleading due to advances in parallel fields.

Finding an alternative to the contemporary distinction between the two icing regimes mentioned is the first and most important aim of this work. This will be accomplished by a consideration of the kinetics of ice crystal growth, allowing for a finite supercooling, Δ_1, at the ice/water interface, relative to T_m. Recent interferometric measurements of the temperature field around ice crystals growing in supercooled water [11] have confirmed this supercooling as a driving force for ice dendrite growth. Experimental relationships between the ice growth rate in the a- or c-axis directions and the appropriate supercooling at the ice/water interface are abundant in the literature. The type of function depends on the mechanism chosen to explain the displacement of the solid/liquid interface, whether 2-D embryo nucleation, edge or screw dislocation growth, or linear growth [12]. Choosing a relationship characterizing linear growth, we will demonstrate that the *application of this relationship alone will specify the water film supercooling*. The solution will be conditioned by assuming the absence of appreciable heat conduction into the already-formed ice deposit on the substrate, and by assuming that the ice/water interface is essentially isothermal. In this way, we differ with some authors, who consider a relationship between ice growth rate and supercooling in water at some finite, but undetermined distance from the interface, referred to as "bath supercooling" or "bulk water supercooling". In order to apply the latter term to the case of a thin supercooled water film flowing on an ice surface, three variables should first be defined:

(i) the temperature profile in the water film,
(ii) the thickness of the film, and,
(iii) either the temperature of the free water surface or the temperature of the ice/water interface.

The temperature of the bulk water may then be defined as the integral of the temperature taken over the entire water film thickness.

1.2. Macroscopic considerations: Interaction of the melt flow and solidification processes

The growth or melting of ice under a water film, typical of icing under high liquid flux conditions, depends not only on the heat exchange with the surroundings, but also on the dynamical conditions in the water film. External and internal factors, such as aerodynamic and gravitational forces, surface tension, etc., lead to water film motion and therefore need to be considered. In this paper, the problem of the interaction of melt flow and solidification processes, which has now been investigated for over 40 years, will be reformulated as a *problem of laminar and turbulent heat transfer through a thin flowing water film from the ice/water interface to the environment*. This is the second important objective of the present paper. We will first consider briefly, however, some solutions to this problem in the closely-related fields of ice physics and metallurgy.

Weertman [13], investigating different mechanisms of water transfer at the base of a glacier, showed that the radius of Röthlisberger channels depends on the heat transfer regime in the water, even more than on other factors investigated. For example, the calculated change in channel radius, when the heat transfer changes from laminar to turbulent, is more than one order of magnitude. Svensson and Omstedt [14] have developed a mathematical upper ocean model, under drifting, melting ice, designed to include the effects of turbulence in the water and discrete roughness elements. The turbulence was modelled with a combination of a low-Reynolds number model close to the ice surface and a high-Reynolds number model at some distance from it. Under the conditions they considered, the turbulent flux of salinity matches the diffusive flux at a distance of 350 μm from the ice surface. For the heat flux, the matching distance was about 1200 μm. This suggests that both turbulent and diffusive fluxes may play an important role, even in very thin liquid films.

[1] It should be noted that a thin *quasi-liquid* skin of supercooled water (with a thickness of the order of a few tens of monomolecular layers) may exist on the surface of ice crystals even under conditions of strong supercooling (down to ~ -15 °C) [6]; more recent treatment of the problem can be found in [7] and [8]. The physical nature of this water skin, however, is quite different from what we are considering here.

In metallurgy, the influence of the flow of the melt on the morphology of a solid has been under scrutiny for several decades. For example, Cole [15] investigated the effect of thermal convective flow on the casting structure by measuring local temperature gradients and temperature fluctuations in the melt. Paradoxically, the highest temperature gradient observed in the laminar sub-layer near the solid/liquid interface was associated with the smallest amplitude of temperature variation. Conversely, the largest amplitude was observed in the upper part of the turbulent thermal boundary layer, where the observed gradient was minimal. Vandenbulcke and Vuillard [16] investigated the influence of natural convection in the melt of an Al–Si eutectic alloy during unidirectional solidification from top to bottom. Measuring the temperature gradient in the fluid and its variation in time, they considered four types of convection: laminar, two intermediate types and turbulent convection. Correspondingly, they were able to identify four different morphological structures in the growing alloys.

In metals, the temperature diffusion boundary layer is thicker than the dynamic boundary layer, while for water the situation is opposite. Such an observation allowed Lighthill [17] to apply a velocity distribution with constant shear for determining heat transfer in the boundary layer. The solution obtained for the case of constant shear, equal to the shear acting at the solid/liquid boundary, was found to be fairly accurate even when applied to other materials with thermal and dynamic boundary layers of the same order of magnitude. This finding supports the adequacy of applying Couette flow for coupled flow and solidification processes. A strong relationship between the nature of the water flow on a cooling plate and the ice shape forming on this plate was revealed in the experiments carried out by Hirata et al. [18,19]. In the case of laminar water flow [18], the accreted ice shape may be represented by a parabolic cylinder developing from the leading edge of the cooling plate. In this region, characterized by accelerating flow, the influence of free stream turbulence is maximal, leading to a discrepancy of about 15% between theoretical and experimental data. For the region where the transition from laminar to turbulent flow occurs, a decrease in ice layer thickness is observed, caused by an increase in the heat transfer coefficient associated with the transition. The transition Reynolds number corresponding to this location was found to be lower than the one where ice does not accrete on the plate. Depending on whether the water flow remains attached or becomes separated, smooth and step transitions were observed, respectively. In both cases, a gradual increase of the ice layer thickness was observed in the subsequent flow in a turbulent heat transfer regime. An analogous effect was observed in channel flows [20]. A reduction of the transitional Reynolds number in the case with an ice-covered substrate, as compared to the case without ice, was also observed in the experiments where the substrate had a cylindrical shape [21]. For a three-component system, including salt in the flowing water, the interaction of natural convection and melting processes is much more complex, depending on temperature and salinity factors [22]. A relation between turbulent water flow and a cusped ice/water interface was observed as well.

1.3. Microscopic consideration: Interaction of the melt flow and dendrite growth processes

In contemporary theories for dendrite growth in the presence of an external flow, the bulk supercooling and the supersaturation, expressed through a combination of the Stefan and Nusselt numbers of the dendrite, St_D and Nu_D, respectively, are usually related to the Péclet numbers of the dendrite, calculated for the fluid flow and dendrite growth velocities, Pe_F and P_D, respectively [23]. The problem of dendrite growth then leads to the determination of temperature and concentration fields around the dendrite under external flow. Two problems arising should be cleared up here: various supercoolings used in the literature and tilted dendrite growth.

The entire supercooling of the melt may be considered as consisting of three main components [24]:

(i) the difference in temperature between the solid/liquid interface at any point and the melt far from this interface, $\Delta_{bk} - \Delta_1$;
(ii) the difference in temperature of the solid/liquid interface between irreversible processes (i.e., with a certain supercooling) and reversible processes (i.e., with the equilibrium temperature for a solid and its melt), Δ_1;
(iii) the difference between the equilibrium temperatures of an appreciably curved and a planar interface should be considered; the curved interfaces we refer to may include the tip of a dendrite or a nucleus, or a bump on the planar interface.

The first supercooling mentioned, which is a prevailing factor at low ice growth rates, controls the dissipation of latent heat, while the second, which becomes comparable to the first only at a high ice growth rate, is responsible for the kinetics of interface processes. The third supercooling component, which generally remains of a lesser order of magnitude than the first two, is a result of the interaction of heat diffusion and capillary processes. Heat diffusion tends to maximize the curvature of the interface and thus minimize the scale of the morphology, while capillary forces tend to minimize curvature of the interface and thereby maximize the scale of morphology. In the case of steady state growth, all three supercoolings should be constant. Following Macklin and Ryan [25], the maximum ice growth rate in quiescent water, G_m, coinciding with the dendrite axis, can be written as a contribution of the growth rate along the a-axis, G_a, i.e., in the basal plane, and along the c-axis, G_c, i.e., in the prismatic plane, respectively:

$$G_m = G_a \cos\varphi + G_c \sin\varphi \tag{I.1}$$

where ϕ is the inclination of the dendrites with respect to the basal plane. It appears from a number of experiments [26] that growth in the basal plane is always faster than in the prismatic plane. It was found also, from natural observation [27] and the experimental investigation [28] of ice frozen from flowing saline water that the c-axis aligns with the direction of flow. Thus, in 2-D considerations of ice growth, the direction of the normal to the ice/water interface will coincide the direction of the a-axis of the growing dendrite. The ice growth rate in this direction in quiescent water, G_a, was the subject of much investigation during the sixties [26], and may be expressed as a function either of bulk water supercooling or supercooling at the ice/water interface [29, 30]:

$$G_a = f(\Delta_{\mathrm{bk}}) \quad \text{or} \quad G_a = f(\Delta_1) \tag{I.2}$$

In the case of flowing water, the first relationship should be modified to include the velocity of the flow $\boldsymbol{u}_F(u, v)$, as was done in the experimental investigation [31]. The shape of the dependence obtained:

$$G_a = f(\Delta_{\mathrm{bk}}, u_F) \tag{I.3}$$

is very similar to that used in the contemporary theories mentioned earlier [23], i.e., $Nu_D = f(St_D, Pe_F, P_D)$, and it may be used preferentially for low supercoolings. The considerations preventing the direct use of such a relationship were expounded at the end of Section 1.1. They are related to the introduction of two integrals taken over the water film thickness, $\Delta_{\mathrm{bk}} = \frac{1}{h}\int_0^h (T_m - T)\,\mathrm{d}y$, and $\bar{u} = \frac{1}{h}\int_0^h u\,\mathrm{d}y$, in the differential equation, called the Stefan condition. Here u is water film velocity distribution. A simplified solution may be obtained, however, if prescribed profiles for both variables are used, or if Δ_2 is substituted for Δ_{bk}. Another way of overcoming the problem is to assume that the relationship $G_a = f(\Delta_1)$ is one of the curves of a family of similar curves for different flow rates. Then, by calculating the temperature and velocity fields in the film, it is always possible to obtain a unique solution $G_a = f(\Delta_1)$ for a prescribed dynamic condition. This last approach is the one used in this investigation.

Another factor to be discussed here is tilted dendrite growth, which was mentioned indirectly at the beginning of this section. From this earlier discussion, one may conclude that the axis of dendrites growing in the flowing melt is inclined to the ice/water interface at an angle of $90° - \varphi$. Tzavras and Wallace [32] investigated the symmetry of steel dendrites grown from flowing melt in a furnace under unidirectional growth. They found that dendrites were "turned" into the flow, when the flow was laminar. Under these circumstances, a partially equiaxed columnar structure was obtained. The symmetry of the growing dendrites, however, was destroyed at a flow speed of about 20–25 cm·s^{-1}, when the flow became turbulent. In turbulent conditions, the flow "bent" the dendrites in random directions, which resulted in random, rounded shapes. As the flow velocity was increased to 50 cm·s^{-1}, a combined thermal and mechanical effect was observed, which resulted in the growth of a fibrous structure with a reduced growth rate, even though the ratio of the temperature gradient to the growth rate was high enough to produce a cellular structure. Tzavras and Wallace inferred that under highly turbulent flow, travelling waves appeared in the diffusion boundary layer.

Several significant theories of dendrite growth in the presence of external forces were revised and experimentally verified [33] by measuring the concentration field around the growing dendrite. It was found that measured supersaturations may be predicted fairly accurately with potential or uniform flow considerations. Tilted dendrite growth in a parallel shear flow of the melt was numerically investigated recently by phase-field simulation [34]. In spite of earlier experimental findings, which suggested that the shape of the tip of the dendrite is not affected by applied melt flow, while the stability parameter is considerably affected by it, this investigation found that melt flow increases asymmetric growth of side branches as the angle between the flow and dendrite growth direction increases. Three different growth regimes were found according to the corresponding contribution to heat transfer from the tip through different processes:

(i) quasi-steady growth controlled by an undisturbed temperature field, where both the Péclet numbers, mentioned earlier, are less than unity;
(ii) diffusion controlled growth, where

$$\max(1, Pe_F, P_D) = P_D$$

(iii) flow controlled growth where convection is the prevailing mechanism for heat transfer, i.e.,

$$\max(1, Pe_F, P_D) = Pe_F$$

Analogous diffusion-convection interaction and its further consequences on the morphology of dendrites were experimentally investigated in earlier research using Couette flow [35]. Both primary and secondary dendrite spacing was found to be affected by the flow of the melt and thus by the interaction between convection and diffusion processes.

Recently, new experimental data have been obtained concerning crystal growth velocity under conditions of "pure" forced convection, [36,37]. These experiments were conducted in such a way as to exclude the effect of thermal convection on the growth rate of crystals, an effect initially observed for ice [38]. All of these experiments present evidence of the strong dependence of crystal growth on the flow of its melt. This is the primary reason for considering a microscopic rather than a macroscopic approach to the understanding of the phenomenon of icing in this paper.

In addition, a microscopic approach makes it possible to examine the instability of the moving interface between the solid (ice) and the supercooled melt (water), under fluctuations of the thermodynamic and dynamical parameters. We start with the supposition that the interrelated initial stability and shape of the interface might be modified by poten-

tial changes in the coefficient of heat transfer in the water film. Natural icing processes always occur under conditions of varying or fluctuating thermodynamic parameters. Hence, it is important to assess the possible impact of external fluctuations, as well as any related internal instabilities, on the growth of the icing interface.

The conclusion to be drawn from this brief review of the literature is that the dynamics of a water film flowing on an icing surface may be the key factor influencing the morphology and growth of the ice deposit. In this paper we will attempt to confirm and elaborate upon this particular finding. An attempt will thus be made to include a microscopic heat balance analysis related to the kinetics of crystal growth, and to elucidate its connection to the macroscopic heat balance, taking into account the dynamics of melt flow.

2. Formulation of the problem and principal assumptions

For simplicity, we will consider a one-dimensional model of icing on a flat plate, We believe, however, that the essential conclusions obtained from such a model will be applicable to more complex geometrical structures. The icing object to be considered is located within a supercooled air–aerosol flow; it is supposed then that a thin water film has formed on the icing surface; and that the layer lying immediately adjacent to the surface of the structure has already turned into ice (Fig. 1). The water film is assumed to flow under the influence of a constant shear stress, F, applied to its surface by the air stream. The supply of water derives from two processes: the inflow of water from upstream along the plate, and the collection of supercooled water droplets on the surface of the water film. The loss of water is also due to two processes: the discharge of water downstream along the plate, and its conversion into ice. The inflow and outflow of the water are of the same order of magnitude; they are, however, much greater than the droplet collection and solidification fluxes, which are smaller, but of the same order of magnitude as each other.

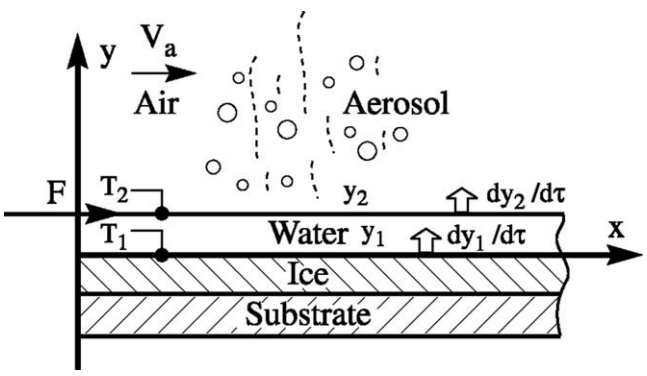

Fig. 1. Schematic of a thin, supercooled water film flowing on the surface of accreted ice in the "wet" regime.

We will consider one of four possible combinations of the laminar and turbulent regimes, for parallel air–aerosol and water film flow. Specifically, we will consider laminar flow in each medium. The exact formulation of the regime in the air–aerosol, which determines the surface temperature of the water film and its conditioning by the free steam turbulence, will be the theme for future research. Here, we consider quasi-steady external thermodynamic conditions, with either constant heat flux or constant temperature conditions at the water surface. Bearing in mind that natural conditions never remain constant, we will consider how short-term changes or fluctuations of one or several thermodynamic parameters result in changes in the thickness of the water film, and influence the rate of ice growth in supercooled flowing water.

For steady, fully-developed, homogeneous flow of a thin water film (i.e., independent of the x-coordinate), with no pressure gradient, the following governing equations for x-momentum and heat transfer hold, in both laminar and turbulent regimes:

$$\frac{\partial}{\partial y}\left\{(\nu_w+\varepsilon_M)\frac{\partial u}{\partial y}\right\}=0 \tag{1}$$

$$\frac{\partial}{\partial y}\left\{(\chi_w+\varepsilon_H)\frac{\partial T}{\partial y}\right\}=\frac{\partial}{\partial y}\left\{\left(\frac{\nu_w}{Pr}+\frac{\varepsilon_M}{Pr_t}\right)\frac{\partial T}{\partial y}\right\}=u\frac{\partial T}{\partial x}+v\frac{\partial T}{\partial y} \tag{2}$$

The properties of water are designated as follows: ν_w and χ_w are the kinematic viscosity and thermal diffusivity, respectively ($m^2\cdot s^{-1}$); ε_M and ε_H are eddy diffusivities for momentum and heat transfer, respectively ($m^2\cdot s^{-1}$); Pr and Pr_t are the molecular and turbulent Prandtl numbers, respectively. Furthermore, $u(y)$ is the tangential component of velocity ($m\cdot s^{-1}$), and $T(x,y)$ is the temperature in the supercooled water film (K). In laminar flow, the eddy diffusivities are omitted. All terms containing the normal component of velocity in the boundary layer have been omitted, since it is negligible in comparison with the tangential component. The right-hand terms in Eq. (2) are retained in order to consider the possibility of convection far from the lower boundary, and to take into account the fact that v, though small, is finite, while the order of magnitude of $\partial T/\partial y$ is unknown.

The following momentum boundary conditions are imposed at the air/water and ice/water interface, respectively:

$$\left.\frac{\partial u}{\partial y}\right|_{y=y_2}=\frac{F}{\rho_w\nu_w} \tag{3}$$

$$u|_{y=y_1}=0 \tag{4}$$

where F is the interfacial shear stress at the free surface of the liquid film ($N\cdot m^{-2}$), and ρ_w is the water density ($kg\cdot m^{-3}$). Let us consider a constant interfacial shear stress, for the ideal case of a fully smooth free surface without surface waves, consistent with the absence of a pressure gradient in the liquid film. While not accounting for surface waves is a possible drawback of the model, it is offset to

some degree by the considerable advantage of having a steady-state model. Nevertheless, the enhanced shear stress produced by the waves, should be taken into account, and will be later. It is clear also that gravity may become significant if the following two conditions are satisfied simultaneously:

(i) the water film thickness is of order of magnitude O (mm); and
(ii) the direction of the film flow forms a certain angle with the horizontal plane.

It should be noted that the influence of gravity is excluded automatically, here, by the way the problem is formulated, but that this in no way implies that gravity is negligible.

For the heat transfer equation, in a laminar regime, the following boundary conditions are imposed at the ice/water interface:

$$-\lambda_w \left.\frac{\partial T}{\partial y}\right|_{y=y_1} = \rho_i L_i \frac{\mathrm{d}y_1}{\mathrm{d}\tau} \tag{5}$$

where ρ_i is the density of the growing ice layer at the interface y_1 (kg·m^{-3}); $\mathrm{d}y_1/\mathrm{d}\tau$ is the rate of displacement of this interface (m·s^{-1}); τ is time (s); L_i is the specific latent heat of freezing of water (J·kg^{-1}) and λ_w is the thermal conductivity of water (W·m^{-1}·K^{-1}).

As stated previously, we assume that the accreted ice layer is thick enough to disregard conduction through it. Ice sponginess is also disregarded in this simplified model, but it can easily be shown that its introduction would not change the main conclusions of this research. Moreover, ice sponginess is additional evidence to support the assumption of an absence of heat conduction in the ice layer [39]. We also ignore any longitudinal temperature gradient along the ice surface. Under these conditions, all released latent heat is directed through the water film to the air stream. The growing crystals behave as "roughness elements" producing early turbulence in the water flow [28], since their growth velocity, in general, exceeds the rate of displacement of a planar interface. Clearly, even in this case, turbulence is absent in the laminar sub-layer near the ice/water interface. It may readily be shown, however, that the tips of the ice crystals can reach far into the buffer layer of the water film, where the velocity distribution for the entire film has the shape of the universal law of the wall. Such an approach was taken by Blackmore and Lozowski [40], for example, in connexion with their model for predicting ice accretion sponginess. In the case of laminar heat and momentum transfer, it is considered that roughness elements have no effect on drag increase. In other words, the ice/water interface is considered to be hydraulically smooth.

A second boundary condition for heat transfer at the air/water interface is imposed, for the following two cases:

(a) constant temperature

$$T|_{y=y_2} = T_2 \tag{6a}$$

(b) constant heat flux

$$\lambda_w \left.\frac{\partial T}{\partial y}\right|_{y=y_2} = \sum_{i=1}^{n} Q_i = \text{const} = Q_{\text{out},s} \tag{6b}$$

where Q_i denotes external heat fluxes at the surface of the water film, while $Q_{\text{out},s}$ is the net surface heat flux. Both conditions (6a) and (6b) must ultimately be specified in terms of the external thermodynamic parameters of the air–aerosol flow. The typical heat balance at the free surface includes three principal terms:

(i) convective heat transfer to the airstream;
(ii) sensible heat of the impinging supercooled droplets; and,
(iii) evaporative heat transfer.

The mass transfer equation at the air/water interface explains the displacement of this interface, normal to the water film flow, due to the flux of incoming water droplets:

$$\frac{\mathrm{d}y_2}{\mathrm{d}\tau} = \frac{w \cdot \overline{E} \cdot V_a}{\rho_w} - C_e \tag{7}$$

where $\mathrm{d}y_2/\mathrm{d}\tau$ is the growth velocity of the water film surface (m·s^{-1}); w is the liquid water content (LWC) of the air–aerosol flow (kg·m^{-3}); $\overline{E}$ is the mean transfer efficiency of the dispersed phase from the aerosol onto the surface of the water film. When F is parallel to the water surface, it is the mean entrainment efficiency. In all other cases, it is the mean collection efficiency; V_a is air speed (m·s^{-1}); and C_e (m·s^{-1}) is a correction for the rate of displacement of the air/water surface arising from evaporation [41].

As stated previously, a supercooling, Δ_1, relative to the fusion temperature, is considered to occur at the ice/water interface:

$$T|_{y=y_1} = T_1 = T_m - \Delta_1 \tag{8}$$

This supercooling is typically a fraction of 1 °C, and, in general, it is only partly accounted for by the Gibbs–Thompson effect. Rather, we see it as the supercooling at the ice/water interface, as investigated in [29,30]. It represents the interface-attachment kinetics involved and constitutes the motive power for ice/water interface growth on a microscopic scale:

$$\frac{\mathrm{d}y_1}{\mathrm{d}\tau} = a \cdot \Delta_1^b = a \cdot (T_m - T_1)^b \tag{9}$$

where a (m·s^{-1}·K^{-b}) and b are empirical constants determined experimentally. Essentially, Eqs. (7) and (9) describe the mass balance, since, as stated above, the order of magnitude of $\mathrm{d}y_1/\mathrm{d}\tau$ and $\mathrm{d}y_2/\mathrm{d}\tau$ is the same, unlike the order magnitude of the inflow and discharge of water.

3. Ranges of the laminar and turbulent flow regimes

The solution of Eq. (1) for the laminar regime, with boundary conditions (3) and (4), is a Couette linear profile:

$$u = \frac{F \cdot y}{\rho_w \nu_w} \tag{10}$$

Integrating this profile over the film thickness, one obtains the mean water film velocity:

$$\bar{u} = \frac{1}{h}\int_0^h u \,\mathrm{d}y = \frac{F \cdot h}{2\rho_w \nu_w} \tag{11}$$

Using $\bar{u}$, one may determine the Reynolds number of the water film as a function of its thickness, Re_F, or the corresponding Reynolds number for flow rate, Re_{FL}:

$$Re_F = \frac{1}{\nu_w}\int_0^h u \,\mathrm{d}y = \frac{\bar{u} \cdot h}{\nu_w} = \frac{Re_{\mathrm{FL}}}{4} = \frac{\Gamma}{\mu_w} \tag{12}$$

where Γ is the mass flow rate per unit of film width ($\mathrm{kg{\cdot}m^{-1}{\cdot}s^{-1}}$). Each of the two Reynolds numbers is distinct from the other as indicated by the factor 4.

In order to understand the results to be presented next, it would be useful to consider the classification of the liquid film flow regimes. Fulford [42] recognizes $Re_F = 270$ as the transition Reynolds number from laminar to turbulent flow in the liquid film. Kutateladze [43] distinguishes four flow regimes: a *stable laminar regime*, whose upper limit is defined in terms of the Archimedes number, Ar, as $Re_F < 2.3 \times Ar^{0.2}$; a *laminar-wavy* regime, extending from this limit to $Re_F = 100$; a *laminar-turbulent transition regime* for $100 < Re_F < 400$; and a *developed turbulent regime* for $Re_F > \sim 400$. Fig. 2 depicts a 3-D representation of the Reynolds number for a water film, calculated by using (12), as a function of the water film thickness and the interfacial shear stress applied at its surface. For the purpose of specifying air and liquid viscosities, the air temperature is taken to be $-10\,^{\circ}\mathrm{C}$, while the water film surface temperature is taken to be $-3\,^{\circ}\mathrm{C}$, the latter being chosen as the mean of measured water film supercoolings on an icing surface [9]. One may conclude from Fig. 2, that, for the ranges of interfacial shear stress and water film thickness considered here, the water film may exhibit all four regimes, passing from perfectly laminar, in the lower left corner, to developed turbulent, in the top right corner. In actuality, the transition to turbulent flow is likely to occur even sooner than Fig. 2 suggests, owing to the fact that the calculated Re_F in the turbulent regime is underestimated as a consequence of using a laminar Couette velocity profile in all the regimes.

A few words must now be said about interfacial shear stress on the water film surface. Shear stress consists of two components, one generated by the airflow and the other by impinging aerosol droplets. Calculations for icing on a cylindrical body [41] have shown that, over a reasonable range of LWC in air under natural conditions ($w < 4 \times 10^{-3}$ $\mathrm{kg{\cdot}m^{-3}}$), the second component is always about one order of magnitude lower than the first. In these calculations, however, the surface of the water film was assumed to be smooth, which is not typically the case under natural conditions. The dominant disturbance wave type, known as *roll waves*, tends to appear on the surface for conditions where the Reynolds number for the water film, Re_F, is of the order of magnitude of several tens. Significant local surface perturbations may also be generated by the impact of the impinging droplets. Since even minor surface perturbation, whatever the cause, have a considerable influence on air shear stress and also increase the interfacial friction factor, the best way to relate interfacial shear stress to airspeed is experimentally. Fig. 3 presents the relationship between the air speed and the resulting interfacial shear stress in a two-fluid-layer flow as a function of water film thicknesses. Calculations were performed using the experimental formula proposed by Cheremisinoff and Davis [44], as follows:

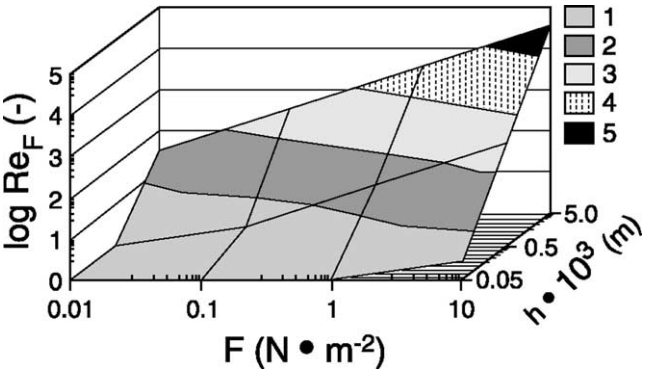

Fig. 2. Reynolds number of a two-dimensional water film, Re_F, as a function of the shear stress applied at its surface, F, and its thickness, h. The computations were made using a Couette laminar profile throughout, even in the laminar–turbulent transition regime, $100 < Re_F < 400$, and the turbulent regime, $Re_F > 400$. The temperature of the surface, T_2, is taken to be $-3\,^{\circ}\mathrm{C}$. The range of air shear stress shown, computed according to the Cheremisinoff and Davis formula [44], covers an air speed range from 1.36 $\mathrm{m{\cdot}s^{-1}}$ to 32.3 $\mathrm{m{\cdot}s^{-1}}$, for $h = 500$ μm and an air temperature $T_a = -10\,^{\circ}\mathrm{C}$.

$$F = f_i \frac{1}{2}\rho_a (V_a - c)^2 \tag{13}$$

where

$$f_i = 0.008 + 2 \times 10^{-5} Re_F \quad \text{for } 100 \leqslant Re_F \leqslant 1700 \tag{14}$$

and f_i is the interfacial friction factor; ρ_a is the air density ($\mathrm{kg{\cdot}m^{-3}}$); and c is the phase speed of surface waves ($\mathrm{m{\cdot}s^{-1}}$). As in the calculation made by Cheremisinoff and Davis, it was reasonably assumed here that $V_a \gg c$ for the interval covered by the Re_F in (14), used in the calculations. As may be seen from Fig. 3, the range of shear stress values presented in Fig. 2 corresponds to the range of natural air speeds during atmospheric icing. The relationship between air speed and shear stress is noticeably different, if the skin friction coefficient c_f is used instead of the interfacial

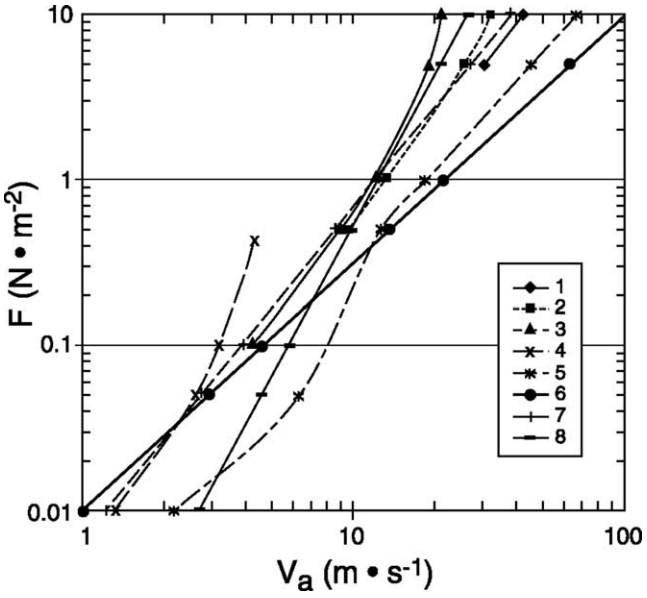

Fig. 3. Surface shear stress as a function of free stream airspeed, over the range considered in Fig. 2. The computations were made according to (13) and (14) for water film thicknesses of: (1) $h = 10^{-4}$ m; (2) $h = 5 \times 10^{-4}$ m; (3) $h = 10^{-3}$ m; (4) $h = 5 \times 10^{-3}$ m. Each curve is computed over an identical range of water film Reynolds number, Re_F. For comparison, corresponding relationships are presented for a flat plate [45]: (5) Schlichting–Prandtl, plate length $l = 1$ m, laminar-turbulent airflow, transition at $F \sim 0.05$ N·m^{-2} with $Re_{a,\mathrm{crit}} = 5 \times 10^5$; (6) Schlichting, $l = 0.1$ m, pure laminar airflow; (7) influence of roughness elements $l/k_s = 500$; (8) air flow over water in a wind-wave tank [47].

friction factor f_i. The skin friction coefficient we refer to is that for airflow along the surface of a smooth, solid flat plate [45], and it takes no account of the features of the water surface. Curves 5 and 6 in Fig. 3 present this relationship for two flow regimes: (5) for transitional-turbulent flow over a plate with a length of $l = 1$ m; (6) for laminar flow over a plate with a length of $l = 0.1$ m. In the first case, transition occurs at $F \approx 0.05$ N·m^{-2}, $u_{\mathrm{crit}} = 6.2$ m·s^{-1}, and $Re_{l,\mathrm{crit}} = 5 \times 10^5$, where the Reynolds number for the plate is calculated according to:

$$Re_l = \frac{V_a \cdot l}{\nu_a} \tag{15}$$

where ν_a is the kinematic viscosity of air.

The average skin friction coefficient for transitional flow, shown in curve 5, may be calculated according to two formulae. Up to the transition point, we use the Schlichting formula for laminar flow:

$$c_{f,l} = \frac{1.328}{\sqrt{Re_l}} \tag{16}$$

Beyond the transition point, we use the Prandtl–Schlichting formula:

$$c_{f,t} = 0.074 Re_l^{-0.2} \cdot \left(1 - \frac{Re_{l,\mathrm{crit}}}{Re_l}\right) + \frac{Re_{l,\mathrm{crit}}}{Re_l} \cdot c_{f,l} \tag{17}$$

As may be seen in curve 6, for the shorter plate, when transition does not occur over the entire range of shear stresses investigated ($u_{\mathrm{crit}} = 62$ m·s^{-1}), and where (16) is used for calculation, the curve lies considerably lower. Comparing curves 5 and 6 with the experimental curves 1 to 4, one may conclude that it is impossible to explain relationships (13) and (14), even by considering the airflow to be turbulent. We can improve the agreement substantially, however, if we use the average skin friction coefficient for a rough, flat plate [45]:

$$\bar{c}_f = \left(1.89 + 1.62 \log \frac{l}{k_s}\right)^{-2.5} \tag{18}$$

where k_s is the height of the roughness elements (m). Curve 7 in Fig. 3, presents the results for $l/k_s = 500$. It lies precisely within the experimental curves. If $l = 0.1$ m, this suggests that the maximum amplitude of interfacial waves, taken to be half the roughness height, would be 10^{-4} m. This value seems quite reasonable for natural conditions [46]. Curve 8 in Fig. 3, presents a possible limit in the relationship between free-stream air velocity and the shear stress created by it at the air-water interface, since it concerns experimental results for airflow over a relatively deep, i.e., 0.5 m, water layer inside a wind-wave tank [47]. The relationship was calculated from an empirical relationship between free-stream air velocity V_a, in the range from 2.4 to 11 m·s^{-1}, and the friction velocity at the air/water interface u_{w-a}:

$$u_{w-a} = 0.02 V_a^{3/2} \tag{19}$$

where Eq. (19) accounts for the presence of turbulence in both air and water.

4. Results and discussion

4.1. Equation for temperature distribution

To continue our investigation of the laminar regime, we need to obtain the temperature distribution through the film, i.e., to solve (2) for the laminar case, using the velocity profile calculated in (10). In order to do this, we will invoke the customary similarity transformation [45] or [48], with the introduction of a new dimensionless coordinate:

$$\eta = \frac{1}{2}\left(u_s y^2 / \nu_w x\right)^{1/2} = \frac{y}{2\nu_w x^{1/2}} \left(\frac{F \cdot h}{\rho_w}\right)^{1/2} \tag{20}$$

where, in place of the free flow velocity at infinity, we have introduced the surface velocity u_s (m·s^{-1}); and h is the water film thickness (m). In order to use the similarity transformation, we account for the fact that the normal component of velocity, v, does exist, even though it is small. Hence, it will be considered in the equations for both momentum and heat transfer. In view of this, we here introduce a stream function for both components of velocity:

$$u = \frac{\partial \psi}{\partial y} \quad \text{and} \quad v = -\frac{\partial \psi}{\partial x} \tag{21}$$

Transforming the stream function, we introduce the new variable:

$$f = \frac{\psi}{(\nu_w \cdot u_s \cdot x)^{1/2}} = \psi \cdot \left(\frac{\rho_w}{x \cdot F \cdot h}\right)^{1/2} \tag{22}$$

Following these transformations, the heat transfer equation (2) may be written:

$$\frac{\mathrm{d}^2 T}{\mathrm{d}\eta^2} + f \cdot Pr \frac{\mathrm{d}T}{\mathrm{d}\eta} = 0 \tag{23}$$

The boundary conditions (6a) and (6b), at the air/water interface, transform as follows:
at

$$\eta = \frac{h}{2}\left(\frac{u_s}{\nu_w x}\right)^{1/2} = \frac{h^{3/2}}{2\nu_w x^{1/2}}\left(\frac{F}{\rho_w}\right)^{1/2}$$

we impose either

(a) constant temperature

$$T = T_2 \tag{24a}$$

or

(b) constant heat flux

$$\frac{\partial T}{\partial \eta} = \frac{2X^{1/2} \cdot Pr}{c_w (Fh\rho_w)^{1/2}} \sum_{i=1}^{n} Q_i \approx \text{const} \quad \text{for } \Lambda \geqslant \Lambda_{\text{lin}} \tag{24b}$$

where $X = (x_1 + x_2)/2$ is an average value of the x-coordinate over the considered interval. The similarity variable Λ and its critical value will be discussed later.

The corresponding transformed boundary conditions at the ice/water interface, (8) and (5), may be written:
(a) constant temperature:

$$\eta = 0, \qquad T = T_1 \tag{25a}$$

(b) constant heat flux:

$$\eta = 0, \qquad \frac{\partial T}{\partial \eta} = \frac{2X^{1/2} \cdot Pr \cdot \rho_i \cdot L_i}{c_w (Fh\rho_w)^{1/2}} \cdot \frac{\mathrm{d}y_1}{\mathrm{d}\tau} \tag{25b}$$

It should be noted that, since the variable η is a function of both the original variables x and y, the transformation of conditions (6b) and (5) into (24b) and (25b), respectively, requires some explanation. The original equation (2), in its laminar form, along with Eq. (5a), implies that the heat generated by viscous dissipation can be transferred by both conduction and convection. As will be seen later, depending on the boundary conditions applied at the upper and lower surfaces of the liquid film, one may obtain cases with various contributions of conduction and convection over different longitudinal length scales. For example, in the unnatural situation of bi-isothermal interfaces, i.e., ice/water and air–aerosol/water, convection is important only near the origin along the x-axis, while it is entirely insignificant at greater distances. This is, in part, why we use an average value, X, instead of x. X is also used because the constant heat flux boundary condition in the initial coordinates becomes a variable heat flux condition in the transformed coordinates. Over a suitable range, x_1 to x_2 centered on X, however, the heat flux may be considered to be essentially constant.

The function f satisfying boundary condition (4) may be expressed as an infinite series in η [48]:

$$f = \frac{\alpha\eta^2}{2!} - \frac{\alpha^2\eta^5}{5!} + \frac{11\alpha^3\eta^8}{8!} - \frac{375\alpha^4\eta^{11}}{11!} + \cdots \tag{26}$$

where the defined constant $\alpha = 1.3282$. Bearing in mind that the solution for the velocity distribution is a Couette linear profile (which is, in fact, a degenerate boundary layer), we return to this approximation by retaining only the first term in (26):

$$\frac{\mathrm{d}^2 T}{\mathrm{d}\eta^2} + \frac{\alpha}{2} Pr\, \eta^2 \frac{\mathrm{d}T}{\mathrm{d}\eta} = 0 \tag{27}$$

The resulting equation (27) can be readily solved analytically by substituting $\frac{\mathrm{d}T}{\mathrm{d}\eta} = \Phi$ and then separating variables. It should be noted that the same result can be obtained, if the stream function is determined with both velocity components satisfying a Couette profile, *viz.* $u = (u_s y/h)$ and $v = (\nu_w y^2/h^3)$, where u_s plays the role of the free stream velocity, and h the role of the degenerate boundary layer thickness. This result was obtained by Levich [48] in solving the convective–diffusion equation.

Eq. (27), together with boundary conditions (24) and (25), make it possible to investigate the relationship between the temperature profile, which arises from the heat transfer from the growing ice/water interface, on the one hand, and the water film thickness and the flow field, on the other. The latter two items are related in a simple fashion through (10). The choice of boundary conditions depends on the scale of the conceptual model of the solidification process with a moving boundary, and the approach used to represent the heat transfer from it. In other words, we need to address the question of what the relationship is, at various length scales, between the two driving influences typically used to describe the displacement of the ice/water interface. In the macroscopic consideration, such as the Stefan solidification problem, the driving influence is the temperature gradient near the solid/melt interface; while, in the microscopic case of ice dendrite growth, it is the supercooling relative to the equilibrium temperature for a solid and its melt. As stated earlier in Section 1.3, this supercooling may, in general, be decomposed into the ice/water interface supercooling and the difference between the interface temperature and the temperature of bulk melt [29], and [30]. The contribution of the components is completely different at various growth rates, which, as was aptly stated in [49], may be a function of both of them. We will first consider the simple instance where the temperatures are constant at both the ice/water and the air–aerosol/water interfaces, thus, drawing a parallel with a thermal boundary layer.

4.2. Bi-isothermal paradigm

A preliminary approximation of the temperature field may be obtained by representing the freezing process,

or displacement of the ice/water interface, as a constant-temperature heat source moving into the water film at a constant velocity as calculated in Eq. (9); here, both interfacial temperatures at y_1 and y_2 are kept constant. This bi-isothermal model is analogous to Couette flow between two plates at temperatures T_1 and T_2. The temperature distribution, at any distance from the origin of the flow, may be found by integrating (27) twice, and then applying (24a) and (25a) to find the constants of integration. The result is:

$$T = T_1 - (T_1 - T_2) \int_0^{\frac{y}{2\nu_w x^{1/2}}\cdot(\frac{F\cdot h}{\rho_w})^{1/2}} \exp\left\{-\frac{\alpha}{6}Pr\eta^3\right\} \mathrm{d}\eta \times \left[\int_0^{\frac{h^{3/2}}{2\nu_w x^{1/2}}\cdot(\frac{F}{\rho_w})^{1/2}} \exp\left\{-\frac{\alpha}{6}Pr\eta^3\right\} d\eta\right]^{-1} \quad (28)$$

By introducing the new variables

$$\Theta = \frac{T_1 - T}{T_1 - T_2} \quad \text{and} \quad \zeta = \eta \cdot \left(\frac{\alpha}{6}Pr\right)^{1/3} \quad (29)$$

one may reduce (28) to the form:

$$\Theta = \int_0^{\zeta_1} e^{-\zeta^3}\,\mathrm{d}\zeta \left[\int_0^{\zeta_2} e^{-\zeta^3}\,\mathrm{d}\zeta\right]^{-1} \quad (30)$$

where

$$\zeta_1 = \frac{y(\frac{\alpha}{6}Pr)^{1/3}}{2\nu_w x^{1/2}} \cdot \left(\frac{F\cdot h}{\rho_w}\right)^{1/2} \quad \text{and}$$

$$\zeta_2 = \frac{h^{3/2}(\frac{\alpha}{6}Pr)^{1/3}}{2\nu_w x^{1/2}} \cdot \left(\frac{F}{\rho_w}\right)^{1/2}$$

The two integrals in (30) may be solved numerically, using data from Abramowitz and Stegun [50]. It is clear from (30), that the values of Θ are confined to the range $0 \leqslant \Theta \leqslant 1$, since:

$$T = T_1 \implies \Theta = 0 \quad \text{and} \quad T = T_2 \implies \Theta = 1 \quad (31)$$

The temperature distribution between two isothermal interfaces is shown in Fig. 4, for several values of the similarity parameter

$$\Lambda = \nu_w \left(\frac{\rho_w x}{F\cdot h}\right)^{1/2}$$

For $\Lambda = 6.3 \times 10^{-5}$ m and $\Lambda = 8.9 \times 10^{-5}$ m (curves 1 and 2, respectively) the main temperature drop is concentrated near the ice/water interface. The heat transfer at these locations near the origin occurs mostly by convection, and the influence of conduction is negligible. For $\Lambda = 2.0 \times 10^{-4}$ m (corresponding to $h = 5 \times 10^{-4}$ m, $F = 1$ N·m^{-2}, and $x/h = 10$), the temperature gradient near the ice/water interface is almost linear, but the gradient near the free surface remains low. For $\Lambda = 2.8 \times 10^{-4}$ m (curve 4) the contribution of convection and conduction are both of the same order of magnitude, while for $\Lambda = 6.29 \times 10^{-4}$ m (curve 5) the contribution of convection has already become negligible. Reaching a critical value, $\Lambda = \Lambda_{\mathrm{lin}} = 8.9 \times 10^{-4}$ m, a linear, conductive temperature profile prevails. Beyond this point:

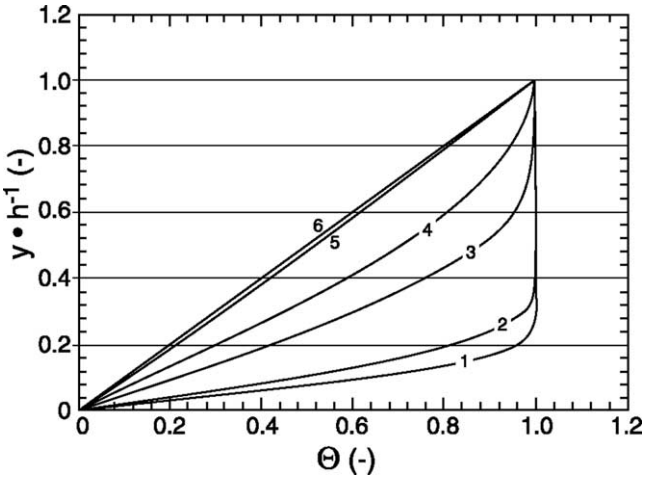

Fig. 4. Distribution of dimensionless temperature $\Theta = (T_1 - T)/(T_1 - T_2)$ through the water film of thickness, h, as a function of the similarity parameter $\Lambda = \nu_w(\rho_w x/F\cdot h)^{1/2}$: (1) $\Lambda = 6.3 \times 10^{-5}$ m; (2) $\Lambda = 8.9 \times 10^{-5}$ m; (3) $\Lambda = 2.0 \times 10^{-4}$ m; (4) $\Lambda = 2.8 \times 10^{-4}$ m; (5) $\Lambda = 6.3 \times 10^{-4}$ m; (6) $\Lambda = 8.9 \times 10^{-4}$ m. For $F = 1$ N·m^{-2} and $h = 5 \times 10^{-4}$ m, the curves correspond to the following distances from the origin of the flow: (1) $x = h$; (2) $x = 2$ h; (3) $x = 10$ h; (4) $x = 20$ h; (5) $x = 100$ h and (6) $x = 200$ h.

$$\Lambda \geqslant \Lambda_{\mathrm{lin}}, \qquad \frac{\partial}{\partial x}\left(\frac{\partial T}{\partial y}\right) \to 0 \quad (32)$$

The greater the shear stress applied at the upper interface, and the thicker the water film, the longer the distance is, over which the temperature profile is nonlinear. The linearization process requires some explanation. According to boundary layer fundamentals, the molecular Prandtl number for water, Pr, is related to the laminar thermal boundary layer thickness, δ_T, and the dynamic boundary layer thickness, δ_D, in the following way:

$$Pr = \frac{\nu_w}{\chi_w} \cong \left(\frac{\delta_D}{\delta_T}\right)^2 \quad (33)$$

For laminar flow, the dynamic boundary layer thickness in water is always greater than the thermal boundary layer, since the kinematic viscosity exceeds the thermal diffusivity. In turbulent flow, however, this asymmetry in the transfer of momentum and heat is appreciably modified, since the eddy diffusivities for momentum transfer, ε_M, and for heat transfer, ε_H, tend to be equalized:

$$Pr_t = \frac{\varepsilon_M}{\varepsilon_H} = \frac{\overline{u'v'}}{\overline{T'v'}} \cdot \frac{\partial T/\partial y}{\partial u/\partial y} \to m \quad (34)$$

where $\overline{u'v'}$ is turbulent "shear stress", a time averaged product of u' and v'; $\overline{T'v'}$ is turbulent heat flux, a time averaged product of T' and v'; while m is some constant close to, but never equal to unity, according to recent

experimental measurements [51]. For water, this constant is $m \cong 0.85$. The total momentum and heat transfers will therefore be dependent on the level of turbulence, taking into account both viscous and turbulent terms. In fully-developed turbulence, where viscous momentum and heat transfer may be disregarded, the thermal and dynamic boundary layers tend to be of a similar thickness. In the case of transitional or developing turbulence, however, these layers will not be the same. The adoption of a Couette linear profile (10) for the velocity distribution over the water film means that the dynamic boundary layer thickness is equal to the water film thickness, $\delta_D \cong h$, and remains constant over all length scales. In contradistinction, the thickness of the thermal boundary layer is not constant, but develops from a minimum defined by (33), to its maximum thickness approximately equal to the water film thickness, $\delta_T \cong h$. Then, once the boundary layer reaches the free surface of the water film, the temperature distribution rapidly becomes linear.

An attempt will be made here to connect the macroscopic scale, on which the solution to (30) is found, with the microscopic scale, on which ice dendrites occur, by applying the results obtained by Kallungal and Barduhn [38]. They reported that the principal radius of curvature of the tip of an ice dendrite, $R_C \cong \mathrm{O}(0.1{-}1\ \mu\mathrm{m})$, is inversely proportional to the bulk supercooling:

$$R_C = C/\Delta_{\mathrm{bk}} \tag{35}$$

where the constant is $C = 0.6 \times 10^{-6}$ m·K, while Δ_{bk} is the supercooling of the bulk water into which the dendrite grows (K). The ice dendrites observed were anisotropic, with a shape, which approximates an elliptical paraboloid having an aspect ratio A:

$$A = \left(\frac{R_2}{R_C}\right)^{1/2} = 10 \tag{36}$$

where R_2 is the secondary radius of the dendrite tip (m). The pronounced anisotropy of ice dendrites suggests that in order to apply macroscopic results, some intermediate scale should be chosen of an order of magnitude of the secondary radius of the dendrite tip, $\mathrm{O}(R_2)$.[2] Now that the scale for the temperature field has been chosen, it is possible, taking into account (29), (35) and (36), to formulate such a field in the following dimensionless form:

$$\frac{\mathrm{d}\Theta}{\mathrm{d}y^+} = \frac{\rho_i L_i R_2}{\lambda_w \cdot (\Delta_2 - \Delta_1)} \cdot \frac{\mathrm{d}y_1}{\mathrm{d}\tau} = \frac{\rho_i L_i A^2 C}{\lambda_w \cdot (\Delta_2 - \Delta_1)\Delta_{\mathrm{bk}}} \cdot \frac{\mathrm{d}y_1}{\mathrm{d}\tau} \tag{37}$$

In (37), the dimensionless temperature gradient is directly proportional to the macroscopic rate of displacement of the ice/water interface. Here, $y^+ = y/R_2$ is the chosen intermediate scale, while $\Delta_2 = T_m - T_2$ is the supercooling at the free surface (K). The bulk water supercooling mentioned earlier is, generally, not a constant, but rather $\Delta_{\mathrm{bk}} = f(\Delta_2, \Delta_1)$.

[2] An investigation on the smallest scale $\mathrm{O}(R_C)$ will be the theme of a future paper.

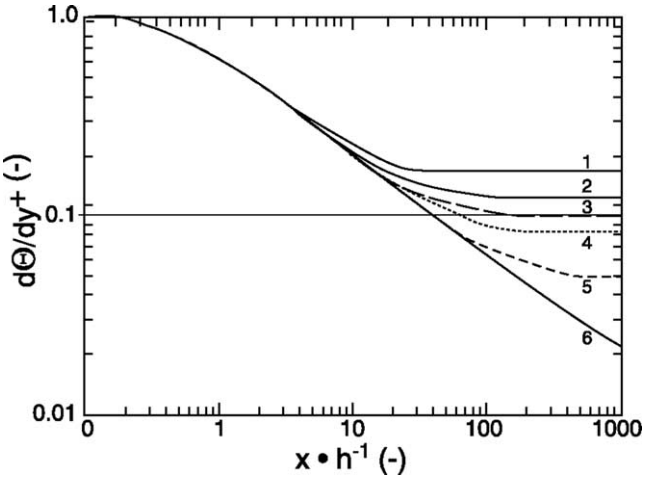

Fig. 5. Dimensionless temperature gradient, $\mathrm{d}\Theta/\mathrm{d}y^+$, in the flowing water film near the ice/water interface, as a function of dimensionless distance from the origin of the flow. The air shear stress is constant $F = 1$ N·m^{-2}. The numbered curves correspond to water film thicknesses of: (1) $h = 300$ μm; (2) $h = 400$ μm; (2) $h = 500$ μm; (4) $h = 600$ μm; (5) $h = 1 \times 10^{-3}$ m; (6) $h = 5 \times 10^{-3}$ m.

Fig. 5 presents the dimensionless temperature gradient for $R_2 \approx \mathrm{const} = 50$ μm, corresponding to $\Delta_{\mathrm{bk}} = 1.2\,^{\circ}\mathrm{C}$, as a function of the dimensionless distance from the flow origin, for several values of water film thickness. A single family of curves emerges, as shown in Fig. 5, when external conditions, defined by the equations for mass transfer (7) and heat transfer (24a) at the free surface, are constant. The case where $F = 1$ N·m^{-2} (curves 1–6) is considered here. Each family of curves may be divided into three distinct regimes. The first is the main stem, which is conditioned by similarity of the solution (30); here, the solutions for all film thicknesses are superimposed. The second regime begins at the location where the thermal boundary layer reaches the free surface, and it is understandable that this location is a function of film thickness, i.e., accepted dynamic boundary layer thickness. The third regime begins at the location where the temperature gradient in the film can be represented as essentially linear.

Fig. 5 also makes it possible to understand the interaction between the growth rate of the ice/water interface and the thickness of the supercooled water film. The type of interaction which occurs is unique to each regime. For the solutions lying along the main stem, a decrease in the water film thickness corresponds to descent down the main stem, i.e., to the right and downward. This implies a corresponding decrease in the ice growth rate. Conversely, an increase in film thickness corresponds to ascent along the main stem, and hence the ice growth rate increases. In other words, the ice/water interface responds in a stable fashion to sudden changes in the water film thickness. If the change in water film thickness or the distance from the flow

origin is sufficiently large, it is possible to reach the second part of the similarity solution. Here, the ice growth rate is unaffected by sudden changes in the water film thickness. In Fig. 5, this corresponds to displacement to the left or to the right with a constant dimensionless temperature gradient $d\Theta/dy^+$. Finally, at the location specified by (32), the third and most important regime is reached. Here, the reaction of the ice/water interface to changes in the water film thickness is unstable. A decrease in the water film thickness, corresponding to displacement to the right and upward along the branches of the similarity stem, is accompanied by an increase in the ice growth rate. Increased ice growth will, in turn, further diminish the water film thickness until it disappears completely. On the other hand, a sudden increase in the water film thickness is accompanied by a decrease in the ice growth rate. In Fig. 5, this corresponds to displacement to the left and downward along the linear branches. Since condition (32) can readily be achieved, it is reasonable to consider a linear temperature profile for the most frequent, naturally occurring cases.

4.3. Linear temperature distribution with close-to-constant surface temperature

Kachurin [52] was the first to conclude that the laminar regime of a shear-driven, supercooled water film, flowing over an accreting-ice surface, is unstable at a sufficiently large distance from the flow origin. Our further examination of this instability will be based on his considerations. For this purpose, a hypothetical equilibrium state is now proposed, where water film thickness and ice growth rate are constant, and the temperatures of the ice/water interface and the water film surface are T_1 and T_2, respectively (Fig. 6). Here, the linear temperature gradient through the film, which governs the ice growth rate, may be written simply:

$$\left.\frac{\partial T}{\partial y}\right|_{y=y_1} = \frac{T_2 - T_1}{y_2 - y_1} \tag{38}$$

Inserting (38) into (5) and taking into account (7) and (9), one obtains:

$$\rho_i L_i \frac{dy_1}{d\tau} + \lambda_w \frac{T_2 - T_m + a^{-1/b}(\frac{dy_1}{d\tau})^{1/b}}{(V_a \cdot w\overline{E}/\rho_w - C_e)\cdot\tau - y_1} = 0 \tag{39}$$

Assuming all external thermodynamic parameters to be constant, (39) is differentiated to obtain the acceleration of the ice/water interface, $d^2y_1/d\tau^2$, taking (7) into account:

$$\frac{d^2y_1}{d\tau^2} = -\frac{dy_1/d\tau(dy_2/d\tau - dy_1/d\tau)}{(y_2 - y_1)[1 + \frac{a^{-1/b}}{b(y_2-y_1)}\cdot\frac{\lambda_w}{\rho_i L_i}(\frac{dy_1}{d\tau})^{(1-b)/b}]} \tag{40}$$

The equilibrium water film thickness may be found by equating the acceleration to zero. This occurs when $dy_1/d\tau$ equals $dy_2/d\tau$:

$$h_{eq} = (y_2 - y_1)_{eq} = \frac{\lambda_w}{\rho_i \cdot L_i \cdot (\frac{V_a \cdot w\overline{E}}{\rho_w} - C_e)} \times \left[T_m - T_2 - a^{-1/b}\cdot\left(\frac{V_a \cdot w\overline{E}}{\rho_w} - C_e\right)^{1/b}\right] \tag{41}$$

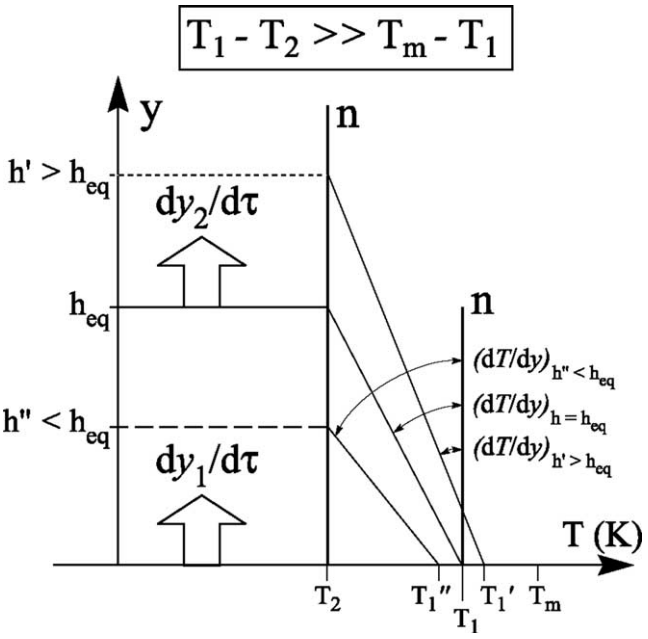

Fig. 6. Schematic of the linear temperature profile, for three different water film thicknesses near a given equilibrium state. An increase in thickness reduces the temperature gradient near y_1, and, as a consequence, the growth rate at the ice/water interface diminishes. Hence, the water film thickness continues to increase. Conversely, a decrease in thickness enhances the growth rate at the ice/water interface, since it steepens the temperature gradient. In this event, the water film disappears rapidly. Consequently, an equilibrium state with a linear temperature gradient over the entire film thickness is unstable.

Let us now imagine that the water film thickness changes due to some sudden disturbance at the ice/water interface. The temperature gradient through the film thickness also changes (Fig. 6), as does the temperature at the ice/water interface. Let us assume, however, that all the external thermodynamic parameters remain constant. We wish to find out how the ice/water interface reacts to the modified water film thickness, after the initial disturbance has been removed. The temperature changes occurring at the ice/water interface are negligible in comparison with the temperature difference between the ice/water and water/aerosol interfaces. Hence, by substitution of (41) into (39), one obtains:

$$\frac{dy_1/d\tau}{(dy_1/d\tau)_{eq}} = \frac{dy_1/d\tau}{dy_2/d\tau} = \frac{h_{eq}}{h} \tag{42}$$

From a comparison of (40) and (42), one may conclude that, if the instantaneous water film thickness is less than the equilibrium water film thickness, the rate of displacement of the ice/water interface exceeds the corresponding equilibrium velocity, and it will continue to increase until the water film has completely disappeared (Fig. 7). Similar unstable behavior of the ice/water interface may be observed if the water film thickness exceeds the equilibrium thickness calculated by (41). In such a case, the rate of displacement of

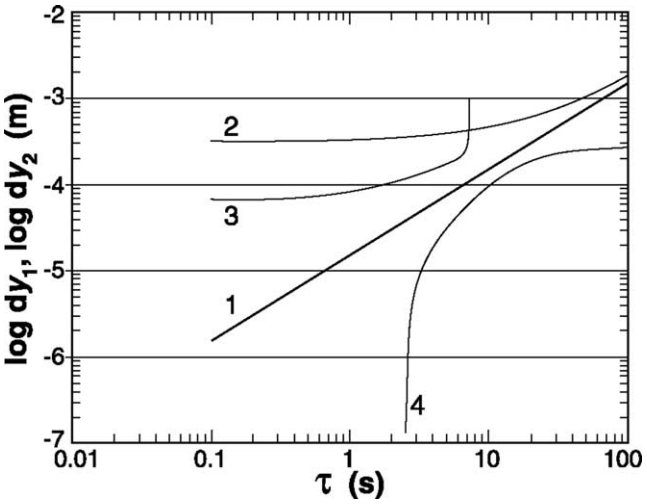

Fig. 7. Displacement of the ice/water interface, in the laminar regime of water film flow, as a function of time under various conditions: (1) equlibrium displacement of the ice/water interface, ($h_{eq} = 317$ μm, $w = 1.2$ g·m^{-3}; $V = 15$ m·s^{-1}); (2) displacement of the free surface; (3) displacement of the ice/water interface with an initial water film thickness $h_0 = 250$ μm; (4) displacement of the ice/water interface with an initial water film thickness $h_0 = 350$ μm.

the ice/water interface will be less than the corresponding equilibrium velocity, and it will continue to decrease until the water film flow becomes turbulent.

4.4. Natural temperature distribution through a water film: Randomly oscillating surface temperature

In the previous two sections it was shown that the laminar supercooled water film flowing on the accreting ice surface is unstable under conditions of constant water-film surface temperature. The following will be an attempt to prove that this conclusion applies to natural laminar water films as well. Experimental data on heat transfer to liquid films flowing on a heated surface will be used to demonstrate this corollary. The most frequent data recorded in this area concern the heat transfer to freely-falling liquid films. These data, therefore, should be considered as a basis for further examination of the stability of the water film and for subsequent application to shear driven water films. In order to present the local heat transfer coefficient in its dimensionless form, it would be useful to introduce several definitions from this area. The linear characteristic of the interaction between gravity and viscosity is the water film thickness, $h_{g\nu}$, defined as follows [43]:

$$h_{g\nu} = \left(\frac{\nu_w^2 \rho_w}{g(\rho_w - \rho_a)}\right)^{1/3} \cong \left(\frac{\nu_w^2}{g}\right)^{1/3} \tag{43}$$

where g is acceleration due to gravity. Both dimensional and dimensionless heat transfer coefficients for a freely-falling liquid film, H (W·m^{-2}·K^{-1}) and H^+, respectively, are defined as follows:

$$H = \frac{Q_{wl}}{(T_2 - T_1)}$$
$$H^+ = \frac{H}{\lambda_w} h_{g\nu} = \frac{Nu}{h/h_{g\nu}} = \frac{Nu}{h^*} = Nu^* \tag{44}$$

where Q_{wl} (W·m^{-2}) is the heat transfer flux from the wall, Nu is the Nusselt number for a water film having a thickness h; while Nu^* is the Nusselt number for a water film having a relative thickness $h^* = h/h_{g\nu}$. Actually, for the definition of heat transfer coefficient, the surface temperature of the film, T_2, is used here, since it invokes experimental data presented by this definition. An analogous heat transfer coefficient based on the temperature of bulk water, T_{bk}, may be defined when T_2 is altered to T_{bk}. In the experimental investigation [53], the common experimental data from this area of heat transfer were presented as follows:

$$H^+ = 1.76 Re_{FL}^{-1/3} \quad \text{for } Re_{FL} \leqslant 2460 Pr^{-0.646} \tag{45}$$
$$H^+ = 3.23 \times 10^{-2} Re_{FL}^{1/5} Pr^{0.344} \quad \text{for } 2460 Pr^{-0.646} \leqslant Re_{FL} < 1600 \tag{46}$$
$$H^+ = 1.02 \times 10^{-3} Re_{FL}^{2/3} Pr^{0.344} \quad \text{for } 1600 \leqslant Re_{FL} < 3200 \tag{47}$$
$$H^+ = 8.71 \times 10^{-3} Re_{FL}^{2/5} Pr^{0.344} \quad \text{for } 3200 \leqslant Re_{FL} \tag{48}$$

These correlations, however, do not distinguish between all laminar and turbulent regimes of water film flow. Only (45) is applicable to the laminar regime where all of the heat transferred from the heating surface is removed from the film surface. In the case where all of the heat is absorbed completely by the film, this relation transforms into:

$$H^+ = 2.27 Re_{FL}^{-1/3} \tag{45a}$$

which is valid for approximately the same range of Reynolds numbers as in the original formula. With reference to the classification of the flow regimes of a liquid film as presented in Section 3, it is also possible to present the heat transfer across the flowing film for the four regimes mentioned in that section. Since the original empirical relations investigated and compiled by Kutateladze [43] are expressed by using the Reynolds number constructed for the film thickness, they may be expressed in a form similar to the one used in (45) through (48), bearing in mind the relationship between the two Reynolds numbers, i.e., Eq. (12). In the *stable laminar regime* (or the asymptotical extension of the Nusselt film concept), the ratio between integral heat transfer and heat conductivity in the vicinity of the solid/liquid interface, i.e., the Nusselt number, is constant:

$$Nu = 1.875, \quad \text{or} \quad H^+ = 2.064 Re_{FL}^{-1/3} \quad \text{for } Re_{FL} \leqslant 9.2 Ar_*^{0.2} \cong 31.5 \tag{49}$$

The water film thickness in this regime may be defined from:

$$h^* = 0.908 Re_{\mathrm{FL}}^{1/3} \tag{50}$$

It may be concluded from the last two expressions that the dimensional coefficient of heat transfer between the solid/liquid interface and the liquid, in this regime, is inversely proportional to the water film thickness $H \sim h^{-1}$.

In a *wavy-laminar regime*, the relationship between the dimensionless heat transfer coefficient and both the Reynolds numbers for the film and flow may be written as follows:

$$H^+ = Nu^* = 1.1 Re_F^{-0.28} = 1.62 Re_{\mathrm{FL}}^{-0.28} \quad \text{for } 31.5 < Re_{\mathrm{FL}} \leqslant 400 \tag{51}$$

The corresponding expression for water film thickness may be written as follows:

$$h^* = 0.817 Re_{\mathrm{FL}}^{1/3} \tag{52}$$

From (51) and (52), one may observe that the inverse proportionality between dimensional heat transfer efficiency and water film thickness weakens in this regime:

$$H \sim Nu/h \sim Re_F^{-0.28} \sim h^{-0.56}$$

In the *laminar-turbulent transition regime*, the heat transfer coefficient and water film thickness may be defined from the following expressions:

$$H^+ = 2.727 \times 10^{-5} Re_{\mathrm{FL}}^{1.18} Pr^{0.4} \quad \text{for } 400 < Re_{\mathrm{FL}} \leqslant 1600 \tag{53}$$

$$h^* = 0.131 Re_{\mathrm{FL}}^{0.6} \tag{54}$$

It may be concluded here, that the relationship between dimensional heat transfer and water film thickness has changed radically from inverse to direct proportionality: $H \sim Re_F^{1.18} \sim h^n$, where $n \cong 1.97$, since the velocity profile is no longer linear.

In the fourth, *developed turbulent* regime, the relationship between heat transfer and the Reynolds number for flow, i.e., water film thickness, weakens to:

$$H^+ = 0.0754 Re_{\mathrm{FL}}^{1/6} Pr^{0.4} \quad \text{for } Re_{\mathrm{FL}} > 1600{-}2000 \tag{55}$$

$$h^* = 0.138 Re_{\mathrm{FL}}^{7/12} \tag{56}$$

In its dimensional form, the relationship between the heat transfer coefficient and the water film thickness also weakens to $H \sim h^{0.286}$.

Fig. 8 presents both series of data mentioned, i.e., that described in (45)–(48) and [53], and that described in (49), (51), (53) and (55) [43], revealing that there is a satisfactory amount of coincidence between them. The boundaries of the regimes in the second series are altered slightly in order to avoid any discontinuity in the values of the heat transfer coefficient. In particular, the transition from the *wavy-laminar* to the *laminar-turbulent transition regime*, in spite of the boundary suggested by (53), occurs in Fig. 8 at a Reynolds number of $Re_{\mathrm{FL,crit}} = 883$. As

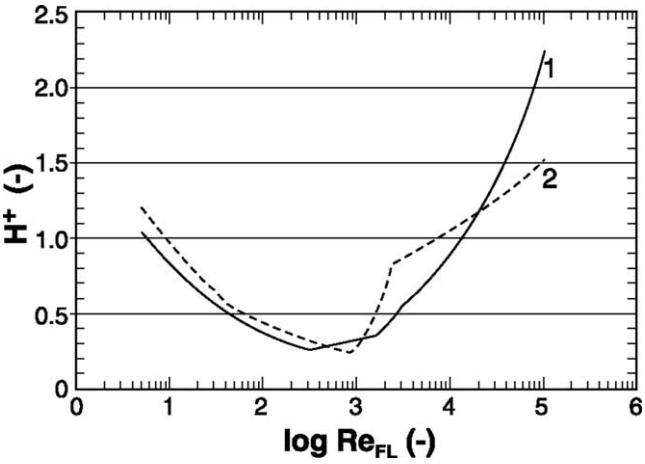

Fig. 8. Dimensionless heat transfer coefficient for various flow regimes according to several authors: (1) formulas (45)–(48) [53]; (2) formulas (49), (51), (53) and (55) [43].

will be seen in the accompanying paper [54], this value is fairly close to the analogous value for transition, obtained from slightly different theoretical considerations. From an examination of Fig. 8, it may be concluded that the heat transfer coefficient is always proportional to some power of the water film thickness $H \sim h^n$. For laminar regimes, it is an inverse proportionality, while for turbulent regimes, it is a direct proportionality. In order to present the results of experiments in the area of heat transfer to freely-falling films in dimensionless form, a multiplication factor is used $h_{g\nu}$. In Appendix A, it is shown that this universal multiplication factor may be employed for shear-driven films as well.

Using definition (29) for substitution in (44), while taking into account the scaling in the y-direction proposed by (35) and (36), for the first laminar regime defined by (49), one may obtain:

$$\frac{\mathrm{d}\Theta}{\mathrm{d}y^+} = 2.064 \left(\frac{\rho_w \nu_w^2 A^2 C}{2F\Delta_{\mathrm{bk}}} \right)^{1/3} \frac{h^{+-2/3}}{h_{g\nu}} = C_\Theta(\Delta_{\mathrm{bk}}) h^{+-2/3} \tag{57}$$

This equation is an analogue of (37). It may be seen, that the temperature gradient is, indeed, inversely proportional to the water film thickness. When water film thickness decreases, the gradient increases and *vice versa*. The dependence, however, is slightly different from that proposed in Section 4.3 by taking a linear approximation with a nearly-constant surface temperature. Defining the equilibrium state of the water film, which is obtained by equating (7) to (9), and performing the same procedure, as in the section mentioned, one obtains the following equation as an analogue of (42):

$$\frac{\mathrm{d}y_1/\mathrm{d}\tau}{(\mathrm{d}y_1/\mathrm{d}\tau)_{\mathrm{eq}}} = \frac{\mathrm{d}y_1/\mathrm{d}\tau}{\mathrm{d}y_2/\mathrm{d}\tau} = \frac{\Delta_2 - \Delta_1}{h^{2/3}} \frac{h_{\mathrm{eq}}^{2/3}}{(\Delta_2 - \Delta_1)_{\mathrm{eq}}} \tag{58}$$

Another equivalent of this law for the first laminar regime may be defined as follows:

$$\left(\frac{\Delta_2 - \Delta_1}{h^{2/3}} \right)_{\mathrm{eq}} = \mathrm{const} \tag{59}$$

This relationship changes just slightly for the second laminar regime. As may be supposed from the relationships presented, the heat transfer in turbulent regimes displays contrary behaviour to that described in this section.

5. Factors causing disturbances in crystallization

Several factors, which can produce sudden disturbances in the crystallization process, will be discussed here. Any disturbance near the crystallization front can be initiated by local thermal heterogeneity produced by either the crystallization front itself or by external influences at the free surface of the water film or by the joint influence both of these factors.

Free convection and the mechanical discontinuity of the solid phase may be counted among factors in the first group, which is conditioned by the processes of diffusion and adsorption of dissolved gases, minerals, ions and macroscopic solid particles at the ice–water boundary. This results in the formation of a layer of heightened concentration near the moving phase boundary. Several thermo-electrical or electrochemical effects as well as diffusion and other processes may be considered consequences of the existence of this layer. Each of them is a potential source of disturbances at the crystallization front. Another source of local disturbance at the ice/water interface is the process of the deposition of admixtures rejected during ice layer formation. This is a result of pre-existing hollowness in the crystallographic structure of ice [55], and the isolation of gases and salt crystals in the water. The capture of entire foreign particles by the ice may be considered as a special source of local temperature disturbance at the crystallization front. This is called *non-equilibrium capture*, and is conditioned by macroscopic defects in the ice structure.

The factors influencing the surface of the flowing water film may be called external factors due to their indirect influence on the stability of the ice/water interface. Here we need to distinguish thermodynamic from mechanical factors, as they are related to the bombardment of the film surface by supercooled water droplets, and their subsequent spreading. Capillary wave formation may be the most important mechanism in this group, giving rise to local disturbances in the temperature gradient near the film surface as a result of wave propagation and differential evaporation. The genesis of microbursts upstream of the crests [56], as well as roughness of the ice/water interface [28], may be factors promoting the early onset of turbulence in the film.

6. Conclusions

The thermodynamic and morphological stability of the crystallization front (i.e., the interface between solid and liquid) under a wind-driven, flowing melt film has been considered as it relates to disturbances of the external thermodynamic parameters, using the ice–water system as an example. The reaction of the ice crystallization front to disturbances of the thermodynamic parameters was especially examined here in connection with laminar flow and heat transfer through the liquid film. In the laminar regime, where the heat transfer from the crystallization front is conditioned only by the adjoining temperature gradient, the reaction of the interface to disturbances of the thermodynamic parameters is always unstable, resulting in corresponding changes in film thickness—either a rapid disappearance of the film, or a rapid thickening of the film until it reaches a stable turbulent regime. As will be seen in the accompanying paper [54], the reaction of the ice/water interface to sudden disturbances in the water film thickness becomes entirely different in turbulent flow.

Acknowledgements

This study was accomplished within the framework of the NSERC/Hydro—Quebec Industrial Chair on Atmospheric Icing of Power Network Equipment (CIGELE) at the University of Quebec in Chicoutimi, in collaboration with the icing group in the Department of Earth and Atmospheric Sciences at the University of Alberta. The authors would like to thank the associates of the CIGELE and an NSERC discovery grant (EPL) for financial support. We are also most grateful to M.L. Sinclair for editorial assistance.

Appendix A. Analogy between shear-driven and gravity-driven films

In the accompanying paper [54], the relation between freely-falling and shear-driven films is investigated. The following connection between two different motive powers for flow is found:

$$\rho_w g = \frac{12}{2^{3/2}} \frac{F^{3/2}}{\mu_w^{1/2} \nu_w^{1/2} Re_{\mathrm{FL}}^{1/2}} = \frac{3F}{h} \tag{A.1}$$

where the final simplified relationship in (A.1) between the two different motive powers was obtained for a linear laminar Couette profile. By substitution of (A.1) in (43), one may define, in analogy with $h_{g\nu}$, the following linear characteristic for interaction between shear stress and viscosity, $h_{\mathrm{SH},\nu}$, having the dimension of length:

$$h_{\mathrm{SH},\nu} = \nu_w \left(\frac{\rho_w^3 Re_{\mathrm{FL}}}{18F^3} \right)^{1/6} = \left(\frac{\nu_w^2 \rho_w h}{3F} \right)^{1/3} \tag{A.2}$$

where the second expression in (A.2) is obtained for laminar flow. Correspondingly, the relationship between the two characteristics, eliminating viscosity, may be defined, using the dimensionless number, $N_{\mathrm{SH},g}$ as:

$$N_{\mathrm{SH},g} = \left(\frac{\nu_w^2 \rho_w^3 Re_{\mathrm{FL}} g^2}{18F^3} \right)^{1/6} = \left(\frac{\rho_w h g}{3F} \right)^{1/3} \tag{A.3}$$

Again, the last expression in (A.3) is obtained for the laminar case. This relationship may be used as a multiplication factor, for transformation from the dimensionless heat transfer coefficient for gravity-driven films, H^+, presented in Fig. 8, to the analogous heat transfer coefficient for shear-driven films, H^+_{SH}:

$$H^+_{SH} = H^+ N_{SH,g} \tag{A.4}$$

Performing this transformation, for example, for (44), one may obtain:

$$H^+_{SH} = 2.064\left(\frac{\nu_w^2 \rho_w^2 g}{6F^2 h}\right)^{1/3} \tag{A.5}$$

The characteristic length (A.2) for this heat transfer coefficient, however, is not constant, as in the case of a gravity-driven film, since it is dependent on the water film thickness.

References

[1] J. Langmuir, K.B. Blodgett, A mathematical investigation of water droplet trajectories, US Army Air Forces Technical Report 5418, 1946.
[2] L.M. Levin, On a deposition of particles from flow on obstacles, Dokl. Akad. Nauk SSSR 91 (1953) 1329–1332.
[3] B.L. Messinger, Equilibrium temperature of an unheated icing surface as a function of air speed, JAS 20 (1953) 29–42.
[4] T.E.W. Schumann, The theory of hailstone formation, Quart. J. Roy. Meteorol. Soc. 64 (1938) 3–21.
[5] F.H. Ludlam, The hail problem, Nebula 1 (1958) 12–96.
[6] N.H. Fletcher, Surface structure of water and ice. II. A revised model, Philos. Mag. 18 (1968) 1287–1300.
[7] J.S. Wettlaufer, M.G. Worster, L.A. Wilen, J.G. Dash, A theory of premelting dynamics for all power law forces, Phys. Rev. Lett. 76 (1996) 3602–3605.
[8] L. Makkonen, Surface melting of ice, J. Phys. Chem. B 101 (1997) 6196–6200.
[9] R. List, F. Garcia-Garcia, R. Kuhn, B. Greenan, The supercooling of surface water skins of spherical and spheroidal hailstones, Atmos. Res. 24 (1989) 83–87.
[10] B.J.W. Greenan, R. List, Experimental closure of the heat and mass transfer theory of spheroidal hailstones, J. Atmos. Sci. 52 (1995) 3797–3815.
[11] I. Braslavsky, S.G. Lipson, Interferometric measurement of the temperature field in the vicinity of ice crystals growing from supercooled water, Phys. A 249 (1998) 190–195.
[12] W.B. Hillig, D. Turnbull, Theory of crystal growth in undercooled pure liquids, J. Chem. Phys. 24 (1956) 914.
[13] J. Weertman, General theory of water flow at the base of a glacier or ice sheet, Rev. Geophys. Space Phys. 10 (1972) 287–333.
[14] U. Svensson, A. Omstedt, A mathematical model of the ocean boundary layer under drifting melting ice, J. Phys. Oceanogr. 20 (1990) 161–171.
[15] G.S. Cole, Temperature measurements and fluid flow distributions ahead of solid–liquid interfaces, Trans. Metall. Soc. AIME 239 (1967) 1287–1295.
[16] L. Vandenbulcke, G. Vuillard, Influence de la convection sur la solidification dirigée de l'alliage eutectique Al–Si. I, J. Cryst. Growth. 12 (1972) 137–144.
[17] M. Lighthill, Contributions to the theory of heat transfer through a laminar boundary layer, Proc. Roy Soc. London Ser. A 202 (1950) 359–376.
[18] T. Hirata, R.R. Gilpin, K.C. Cheng, E.M. Gates, The steady state ice layer profile on a constant temperature plate in a forced convection flow—I. Laminar regime, Internat. J. Heat Mass Transfer 22 (1979) 1425–1433.
[19] T. Hirata, R.R. Gilpin, K.C. Cheng, The steady state ice layer profile on a constant temperature plate in a forced convection flow—II. The transition and turbulent regimes, Internat. J. Heat Mass Transfer 22 (1979) 1435–1443.
[20] B. Weigand, H. Beer, Ice-formation phenomena for water flow inside a cooled parallel plate channel: An experimental and theoretical investigation of wavy ice layer, Internat. J. Heat Mass Transfer 36 (1993) 685–693.
[21] K.C. Cheng, H. Inaba, R.R. Gilpin, An experimental investigation of ice formation around an isothermally cooled cylinder in crossflow, J. Heat Transfer 103 (1981) 733–738.
[22] E. Josberger, S. Martin, A laboratory and theoretical study of the boundary layer adjacent to a vertical melting ice wall in salt water, J. Fluid Mech. 111 (1981) 439–473.
[23] M. Kind, W.N. Gill, R. Ananth, The growth of ice dendrites under mixed convection conditions, Chem. Engrg. Comm. 55 (1987) 295–312.
[24] B. Chalmers, Principles of Solidification, Robert E. Krieger Publishing Company, Malabar, FL, 1982.
[25] W.C. Macklin, B.F. Ryan, Growth velocities of ice in supercooled water and aqueous solutions, Philos. Mag. 17 (1968) 83–87.
[26] H.R. Pruppacher, J.D. Klett, Microphysics of Clouds and Precipitation, D. Reidel Publishing Company, Dordrecht, 1978.
[27] W.F. Weeks, A.J. Gow, Crystal alignments in the fast ice of Arctic Alaska, J. Geophys. Res. C 85 (2) (1980) 1137–1146.
[28] P.J. Langhorne, W.H. Robinson, Alignment of crystals in sea ice due to fluid motion, Cold Reg. Sci. Technol. 12 (1986) 197–214.
[29] H.R. Pruppacher, Interpretation of experimentally determined growth rates of ice crystals in supercooled water, J. Chem. Phys. 47 (1967) 1807–1813.
[30] W.C. Macklin, B.F. Ryan, Interpretation of the growth rates of ice dendrites in supercooled water, J. Chem. Phys. 50 (1969) 551–552.
[31] R. Fernandez, A.J. Barduhn, The growth of ice crystals, Desalination 3 (1967) 330–342.
[32] A.A. Tzavras, J.F. Wallace, Cast steel structures grown under fluid flow, J. Cryst. Growth 13/14 (1972) 782–786.
[33] V. Emsellem, P. Tabeling, Experimental study of dendritic growth with an external flow, J. Cryst. Growth 156 (1995) 285–295.
[34] R. Tönhardt, G. Amberg, Phase-field simulation of dendritic growth in a shear flow, J. Cryst. Growth 194 (1998) 406–425.
[35] Tao Huang, Lu Deyang, Zhou Yaohe, Diffusion–convection effects on constrained dendritic growth in dilute alloys, Acta Astron. 17 (1988) 997–1002.
[36] Y.W. Lee, R. Ananth, W.N. Gill, Selection of a length scale in unconstrained dendritic growth with convection in melt, J. Cryst. Growth. 132 (1993) 226–230.
[37] Y. Miyata, H. Tanaka, Dendritic growth in undercooled melt with forced convection: Experiment for pure succinonitrile, ISI J. Internat. 35 (1995) 596–599.
[38] J.P. Kallungal, A.J. Barduhn, Growth rate of an ice crystal in subcooled pure water, AIChE J. 23 (1977) 294–303.
[39] L. Makkonnen, Salinity and growth rate of ice formed by sea spray, Cold Reg. Sci. Technol. 14 (1987) 163–171.
[40] R.Z. Blackmore, E.P. Lozowski, A theoretical spongy spray icing model with surficial structure, Atmos. Res. 49 (1998) 267–288.
[41] A. Karev, Thermodynamic and radiolocation properties of icing surfaces, Ph.D. Thesis, Russian State Hydrometeorological Institute, St. Petersburg, Russia, 1993.
[42] G.D. Fulford, The flow of liquids in the thin films, Adv. Chem. Engrg. 5 (1964) 151–236.
[43] S.S. Kutateladze, Heat Transfer and Hydrodynamic Resistance Handbook, Energoatomizdat, Moscow, 1990.
[44] N.P. Cheremisinoff, E.J. Davis, Stratified turbulent–turbulent gas–liquid flow, AIChE J. 25 (1979) 48–56.

[45] H. Schlichting, Boundary-Layer Theory, 6th Edition, McGraw–Hill, New York, 1968.
[46] K.J. Chu, A.E. Dukler, Statistical characteristics of thin, wavy films: Part II. Studies of substrate and its wavy structure, AIChE J. 20 (1974) 695–706.
[47] S. Komori, R. Nagaosa, Y. Murakami, Turbulence structure and mass transfer across a sheared air–water interface in wind-driven turbulence, J. Fluid Mech. 249 (1993) 161–183.
[48] V.G. Levich, Physicochemical Hydrodynamics, Prentice–Hall, New York, 1962.
[49] W.C. Macklin, B.F. Ryan, Comment on "Different interpretations of the growth rates of ice dendrites in supercooled water", J. Chem. Phys. 52 (1970) 3854–3855.
[50] M. Abramovitz, A. Stegun, Handbook of Mathematical Functions, 9th Edition, Dover, New York, 1970.
[51] W.M. Kays, Turbulent Prandtl number—Where are we?, J. Heat Transfer Trans. ASME 116 (1994) 284–295.
[52] L.G. Kachurin, On airplane icing theory, Izv. Akad. Nauk SSSR, Ser. Geofiz. 6 (1962) 823–832.
[53] T. Fujita, T. Ueda, Heat transfer to falling liquid films and film breakdown—I. Subcooled liquid films, Internat. J. Heat Mass Transfer 21 (1978) 97–108.
[54] A.R. Karev, M. Farzaneh, E.P. Lozowski, Character and stability of a wind-driven supercooled water film on an icing surface—II. Transition and turbulent heat transfer, Internat. J. Therm. Sci., submitted.
[55] P.V. Hobbs, Physics of Ice, Clarendon Press, Oxford, 1974.
[56] C. Lorencez, M. Nasr-Esfahany, M. Kawaji, Turbulence structure and prediction of interfacial heat and mass transfer in wavy-stratified flow, AIChE J. 43 (1997) 1426–1435.